

X-RAY DETECTION OF THE INNER JET IN THE RADIO GALAXY M84

D. E. HARRIS

Smithsonian Astrophysical Observatory, 60 Garden Street, Cambridge, MA 02138; harris@cfa.harvard.edu

A. FINOGENOV

Max-Planck-Institut für extraterrestrische Physik, Giessenbachstrasse, D-85748 Garching, Germany; alexis@xray.mpe.mpg.de

A. H. BRIDLE

National Radio Astronomy Observatory, 520 Edgemont Road, Charlottesville, VA 22903-2475; abridle@nrao.edu

M. J. HARDCASTLE

Department of Physics, University of Bristol, Tyndall Avenue, Bristol BS8 1TL, UK; m.hardcastle@bris.ac.uk

AND

R. A. LAING

University of Oxford, Department of Astrophysics, Nuclear and Astrophysics Laboratory, Keble Road, Oxford OX1 3RH, UK; rlaing@astro.ox.ac.uk

Received 2002 April 19; accepted 2002 July 24

ABSTRACT

During the course of an investigation of the interaction of the radio galaxy M84 and its ambient cluster gas, we found excess X-ray emission aligned with the northern radio jet. The emission extends from the X-ray core of the host galaxy as a weak bridge and then brightens to a local peak coincident with the first detectable radio knot at $\approx 2''.5$ from the core. The second radio knot at $3''.3$ is brighter in both radio and X-ray. The X-ray jet terminates $3''.9$ from the core. Although all the evidence suggests that Doppler favoritism augments the emission of the northern jet, it is unlikely that the excess X-ray emission is produced by inverse Compton emission. We find many similarities between the M84 X-ray jet and recent jet detections from *Chandra* data of low-luminosity radio galaxies. For most of these current detections, synchrotron emission is the favored explanation for the observed X-rays.

Subject headings: galaxies: active — galaxies: individual (M84) — galaxies: jets — radiation mechanisms: nonthermal — radio continuum: galaxies — X-rays: galaxies

1. INTRODUCTION

The radio galaxy M84 is a low-luminosity (FR I type) radio galaxy in the Virgo Cluster. We obtained *Chandra* observations in order to study the interaction of the radio structures with the hot intracluster medium (ICM), and that work was reported in Finoguenov & Jones (2001). In this paper we report on X-ray emission detected from the inner 300 pc of the northern radio jet.

X-ray emission from radio jets presents us with the problem of identifying the emission process, but once this process is determined, we can then obtain new constraints on physical parameters (Harris & Krawczynski 2002). With the introduction of the relativistic beaming model of Celotti et al. (2001) and Tavecchio et al. (2000), most X-ray emission from jets has been interpreted as indicating either synchrotron emission or inverse Compton scattering off the cosmic microwave background (CMB). For M84, we show that synchrotron emission is the probable process, as has been found for a number of other FR I radio galaxies (Worrall, Birkinshaw, & Hardcastle 2001; Hardcastle, Birkinshaw, & Worrall 2001). The implications of the detected X-ray emission are discussed in § 5.

We take the distance to the Virgo Cluster to be 17 Mpc, so that $1''$ corresponds to 82 pc. We follow the usual convention for flux density, $S \propto \nu^{-\alpha}$.

2. X-RAY DATA

The X-ray data were obtained with the ACIS-S detector on the *Chandra Observatory* (observation ID 803, 2000 May

19). The exposure time was 30 ks, and after filtering for high background, a live time of 28.7 ks was realized. The central X-ray point source is coincident with the position of the radio nucleus. Its spectrum is well described as an absorbed [$N_{\text{H}} = (2.7 \pm 0.3) \times 10^{21} \text{ cm}^{-2}$] power law ($\alpha = 1.3 \pm 0.1$) with a corresponding luminosity of $4 \times 10^{39} \text{ ergs s}^{-1}$ in the 0.5–10 keV band. Further details of the data and basic processing can be found in Finoguenov & Jones (2001).

For image display purposes, we limited the energy range to 0.3–2 keV and binned the data by a factor of $\frac{1}{5}$ to obtain images with pixel size $0''.098$. Various Gaussian smoothing functions were then convolved with the data, and one example is shown in Figure 1; a radio image with X-ray contours superposed. The coincidence of radio and X-ray emission for knots N2.5 and N3.3 is evident (we name these features according to their angular distance from the core in arcseconds). The emission to the southwest of the core at about the same brightness level as the northern jet does not correspond to any radio emission and is part of the complex thermal emission described by Finoguenov & Jones (2001). The data presented there reveal an H-shape for the diffuse component, anticorrelated with radio emission. Furthermore, the asymmetry in the X-ray emission, as well as in the radio, is attributed to hydrodynamic effects caused by the motion of M84 toward the northwest through the hot gas of the Virgo Cluster. As is clearly seen from their large-scale map, the western component of the X-ray emission is more compressed than the eastern one, and in addition is bent toward the south. The southwest enhancement in the X-ray emission, seen in Figure 1, is attributed to the stronger interac-

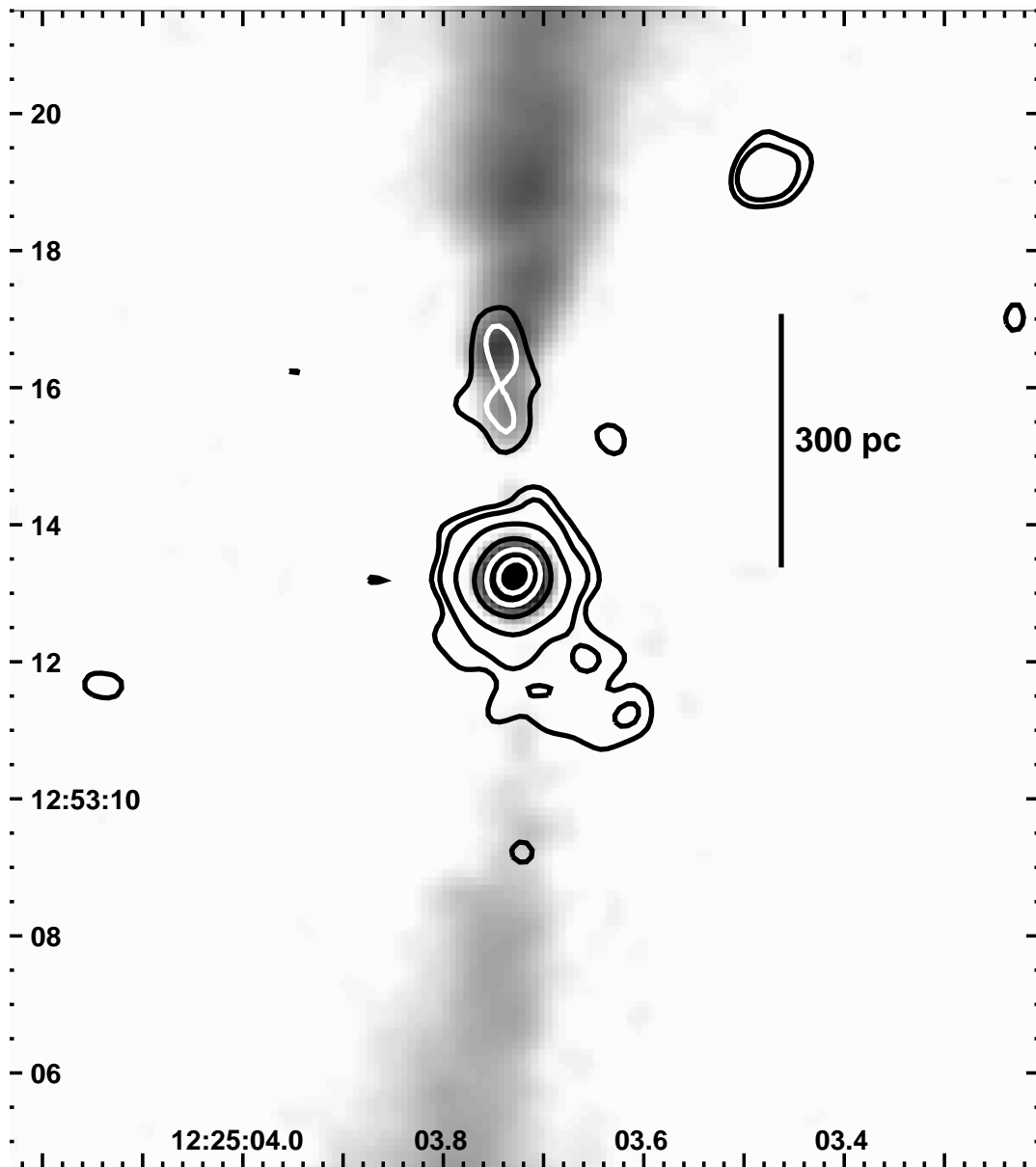


FIG. 1.—Plot of a 5 GHz VLA gray-scale image (restoring beam of $0''.4$) with X-ray contours of the inner region of M84. The X-ray image has been smoothed with a Gaussian of $\text{FWHM} = 0''.5$ and shifted by $0''.09$ in R.A. to align the core with the radio nucleus. A few contours have been changed from black to white to improve visibility. The contour levels are 0.35, 0.5, 1, 2, 3, and 4 counts pixel^{-1} . Since the pixel size is $0''.0984$, these levels should be multiplied by 103.3 to obtain counts arcsec^{-2} . The X-ray detections N2.5 and N3.3 coincide with the first two radio features in the northern jet. The 2σ feature $4''$ to the south of the nucleus (a single contour) contains 10 ± 5 net counts. The scale bar shows the length of 300 pc at the distance of M84.

tion between the ambient hot plasma and the southern radio lobe on the side of maximal compression of the X-ray-emitting plasma.

For an estimate of the spectral parameters, a thermal (Mewe-Kaastra-Liedahl) spectrum was fitted to a large region near the north jet. Then, with the counts extracted from a circle of radius $2''.5$ that included both N2.5 and N3.3, a two-component model was fitted with the temperature and metallicity of the thermal component fixed to that found for the adjacent hot gas (0.55 ± 0.05 keV), but with the amplitudes of both the power law and the thermal components left as free parameters (as was the power-law index). The quantity N_{H} was always fixed to the Galactic value.

A single-component fit to the jet spectrum, allowing only the normalization to vary, gives an unacceptable χ^2 : 51.3 for 16 degrees of freedom. The introduction of an additional component, such as the power law, reduces the χ^2 to an acceptable level of 13.5 per 14 degrees of freedom, and the additional component is statistically significant at the 3.9σ level (or 99.992%). If the second component is modeled with a thermal spectrum instead of a power law, and only the temperature and normalization are allowed to vary, the fit is equally acceptable (13.9/14) and has a temperature of 3.2 ± 1.1 keV and normalization of $(8.7 \pm 3.3) \times 10^{-6}$ in XSPEC units.

The results for the thermal background/power-law jet are shown in Figure 2. From this fit, we find that the power-

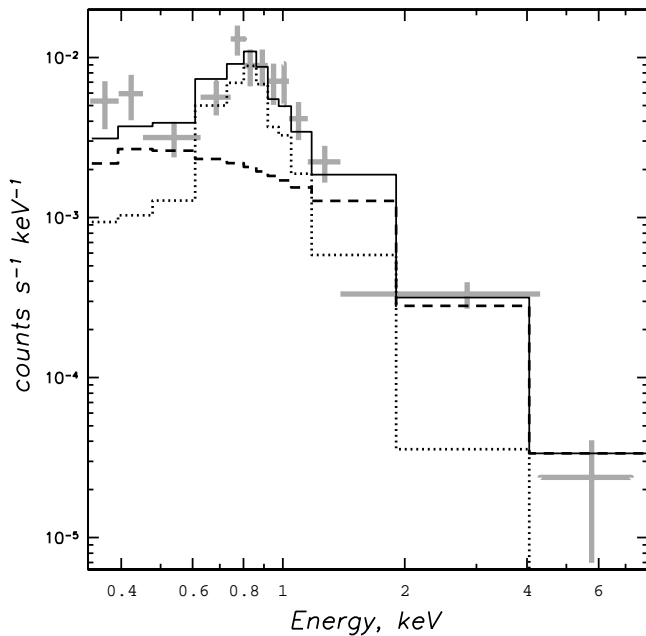


FIG. 2.—X-ray spectrum of emission extracted using a 2.5 diameter circle, centered on the north X-ray jet. Crosses indicate the *Chandra* data, the dotted line shows the contribution of the thermal component from the diffuse emission of M84, the dashed line indicates the power-law spectrum of the jet, and the solid line corresponds to the sum of the two components.

law component has a flux $f(0.3\text{--}7\text{ keV}) = 1.5 \times 10^{-14}$ ergs $\text{cm}^{-2}\text{ s}^{-1}$ and $\alpha = 0.8 \pm 0.3$. This flux corresponds to 42 net counts in our data. Dividing the observed flux according to the ratio of the counts in two small circles centered on the two knots provides the intensity values reported in Table 1.

3. RADIO DATA

The Very Large Array (VLA) data are a combination of observations made in three VLA configurations at 4.9 GHz: in the A configuration on 1980 November 9, in the B config-

TABLE 1
INTENSITY MEASUREMENTS FOR THE CORE AND KNOTS OF M84

Parameter	N2.5	N3.3
Net counts ^a	15 ± 5	28 ± 6
$f_X(0.3\text{--}7\text{ keV})$ (10^{-14} ergs $\text{s}^{-1}\text{ cm}^{-2}$) ^b ..	0.53 ± 0.18	0.96 ± 0.20
$L_X(0.3\text{--}7\text{ keV})$ (10^{38} ergs s^{-1})	1.8 ± 0.6	3.3 ± 0.7
$S(1\text{ keV})$ (nJy)	0.63 ± 0.21	1.15 ± 0.25
$S(5\text{ GHz})$ (mJy) ^c	3.5 ± 0.6	13 ± 3

^a The X-ray intensity of the knots comes from the spectral modeling, but the listed counts come from small circles: $r = 0.35$ for N2.5 and $r = 0.5$ for N3.3. This was done because the two knots are not well separated, being only 0.8 apart. Obviously, the net counts in these small circles do not represent the total counts attributable to the knots, but their sum is close to the 42 counts contributing to the power-law component of the spectral fit within a circle of radius 2.5. Listed uncertainties are the square root of the total counts within the measuring aperture, but they should be augmented by a few counts because of the uncertainty in the appropriate background level to use at the location of the knots.

^b The X-ray flux has been corrected for Galactic absorption, and a power law with $\alpha = 0.8$ was used for both components.

^c The radio flux densities were measured with a variety of AIPS tools.

uration on 1981 June 25, and in the C configuration on 1981 November 17. They were reduced in the AIPS software package using standard self-calibration and imaging methods. The asymmetry in brightness between the northern and southern jets supports the notion that the northern jet is the one coming toward us and that Doppler favoritism is operating out to $\approx 15''$ (1.2 kpc). We do not have radio data of sufficient spatial resolution at lower frequencies to determine accurate spectral indices, but the lower resolution data indicate values of $\alpha \approx 0.65$.

4. PARAMETERS FOR EMISSION MODELS

To estimate physical parameters associated with various X-ray emission mechanisms, we need to assign volumes for the knots. For each knot, we choose a cylindrical volume with a length of 0.8 and radii of 0.15 (N2.5) and 0.21 (N3.3). The overall spectrum for N3.3 is shown in Figure 3.

4.1. Thermal Bremsstrahlung Emission

In many instances (e.g., Harris, Carilli, & Perley 1994), it has been argued that if X-ray emission from radio features were to be from hot gas rather than a nonthermal mechanism, then the required electron densities together with the (equipartition) magnetic field strengths would predict departures from the λ^2 relation of the radio polarization position angle, as well as excess depolarization. Since these effects have not been found, it appears that whatever thermal gas is present in radio-emitting volumes must have a density much lower than that needed to produce the observed X-ray emission. However, there could be excess hot gas around the jet, since we do not have a sufficient resolution or signal-to-noise ratio (S/N) to determine the precise distribution of the emission, and we do not have Faraday-rotation estimates on the arcsecond scales under discussion here.

The X-ray luminosity for each knot is of the order of 10^{38} ergs s^{-1} (Table 1), and the density required to produce this emission from the cylindrical volumes would be 5 cm^{-3} . The masses of the emitting cylinders would be 4 and $7 \times 10^3 M_\odot$ (N2.5 and N3.3, respectively). Assuming a temperature of

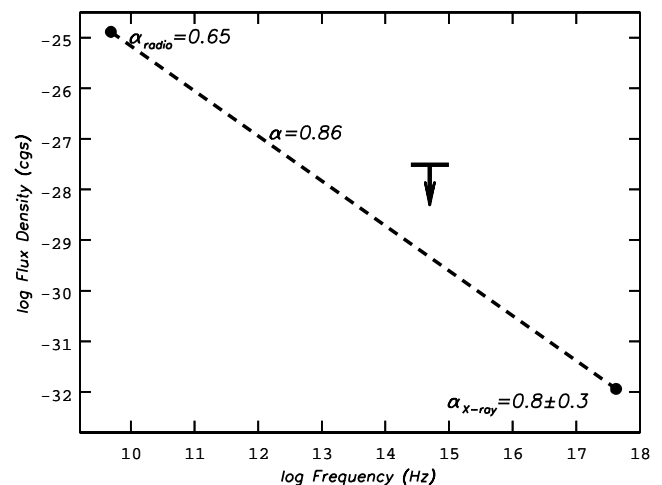


FIG. 3.—Spectrum of knot N3.3 (knot N2.5 is quite similar). The optical upper limit is from archival *Hubble Space Telescope* data: $30\text{ }\mu\text{Jy}$ at 5×10^{14} Hz. The other two points are from Table 1.

1 keV means that the pressure would be 1.6×10^{-8} dynes cm^{-2} . Although this pressure is significantly larger than that expected from the ambient hot gas (3.7×10^{-10} dynes cm^{-2} ; Finoguenov & Jones 2001), since these emitting volumes are well inside the galaxy, there could be additional pressure contributed by cooler gas that does not produce X-rays.

The X-ray spectral analysis (§ 2) demonstrates clear evidence for either a nonthermal or a 3 keV component not seen in nearby regions. In Figure 2, note the excess both below 0.5 keV and above 2 keV. We favor the nonthermal alternative because even adiabatic compression of the X-ray emitting gas to the required densities ($\geq 1 \text{ cm}^{-3}$) should result in a temperature of 15 keV, much higher than what is observed.

4.2. Synchrotron Emission

Even though we do not know the details of the spectrum, we can estimate the synchrotron parameters necessary to produce the observed X-rays with a spectrum such as that shown in Figure 3. For the radio emission from N3.3 (10^7 – 10^{11} Hz), the log of the luminosity would be 38.24 ergs s^{-1} , and the equipartition field would be 111 μG . For a synchrotron X-ray model, we need to extend the spectrum up to 10^{18} Hz with the spectral index $\alpha = 0.9$. In this case, the log of the luminosity would be 39.14 ergs s^{-1} , and the equipartition field would be 143 μG . If the synchrotron emission from N2.5 and N3.3 is mildly beamed (as we argue below), both these luminosity and magnetic field strength estimates should be reduced somewhat.

Although the change required by the extension of the synchrotron spectrum in the total energy contained in the source is not large, the power-law distribution of electron energy would have to extend to $\gamma = 4 \times 10^7$ with a half-life of 10 yr for electrons of this energy. If $\alpha(\text{radio}) = 0.65$, then the spectrum would most likely be a broken power law, but this does not make much difference to the rough estimates calculated here.

4.3. Inverse Compton Emission

The synchrotron self-Compton model fails because the photon energy density is so low that the predicted 1 keV flux density would be 4 orders of magnitude below that observed (assuming an equipartition field of 93 and 111 μG for N2.5 and N3.3, respectively). Inverse Compton (IC) scattering off the CMB photons would require a magnetic field strength of 0.1 μG , more than a factor of 1000 below the equipartition field.

If we invoke relativistic beaming to produce the observed X-ray jet (so that the CMB energy density would be increased by Γ^2 in the jet frame, where Γ is the Lorentz factor of the relativistic jet), an angle between the jet velocity vector and the line of sight would have to be 3° or less, and the beaming factor and Γ would be ≈ 20 . These values, derived from the equations in the Appendix of Harris &

Krawczynski (2002), are inconsistent with estimates from the radio data. From the observed ratio of the intensities of the inner radio jets (i.e., 16 at $3''$ from the core), the angle between the line of sight and the north jet has to be less than 70° and is most likely greater than 45° , since we see the two sides of the jet and lobes well separated. This range in angles corresponds to beaming factors in the range 0.6–1.25 and jet fluid velocities $\beta (=v/c)$ in the range 1–0.6.

5. DISCUSSION

We believe the evidence favors synchrotron emission for the observed X-rays, although to sustain this model, higher S/N X-ray data and optical detections are required. Undoubtedly, there are bulk relativistic velocities in the jet producing the observed intensity differences between the north and south jets, but with velocity vectors not too far from the plane of the sky, we see only mild boosting, and the parameters for IC/CMB emission are completely at odds with all other evidence. To check the “mild beaming” synchrotron model, we note that the ratio of the net counts in the north jet ($r = 1''05$ aperture) to that found in the same sized circle at the same distance to the south is more than 4.1 (where we used the 2σ upper limit for the south value). Thus, the X-ray ratio (north/south) is consistent with the radio value (16) measured at the same distance from the core ($3''$).

Even in fields of the order of 100 μG , the half-life for electrons producing X-rays is so short that they could travel no more than ≈ 3 pc from their acceleration region. Thus, the X-rays clearly demarcate that sort of acceleration region.

The M84 jet is considerably weaker than other FR I galaxy detections. The X-ray luminosity is ≈ 6 times less than that of Cen A, the jet with the lowest luminosity listed in a table of seven FR I jets in Harris, Krawczynski, & Taylor (2002). The combined flux densities of N2.5 and N3.3 are a factor of 84 less than that from knots HST-1 and D in the M87 jet (Marshall et al. 2002); these two knots are within $3''$ of the nucleus of M87, although their physical distance from the core may be larger than that for the M84 knots owing to a larger projection effect. Although some of the disparity in X-ray luminosity between M84 and the other FR I jets may be caused by differences in beaming factors, most of the current sample are believed to have rather large angles between the line of sight and the jet axis, and thus beaming is generally moderate to low in all of them.

We thank the referee for suggestions that led to improvements in the presentation. This work was partially supported by NASA grants and contracts GO0-1145X, GO1-2135A, and NAS 8-39073. The National Radio Astronomy Observatory is a facility of the National Science Foundation operated under cooperative agreement by Associated Universities, Inc.

REFERENCES

- Celotti, A., Ghisellini, G., & Chiaberge, M. 2001, MNRAS, 321, L1
 Finoguenov, A., & Jones, C. 2001, ApJ, 547, L107
 Hardcastle, M. J., Birkinshaw, M., & Worrall, D. M. 2001, MNRAS, 326, 1499
 Harris, D. E., Carilli, C. L., & Perley, R. A. 1994, Nature, 367, 713
 Harris, D. E., & Krawczynski, H. 2002, ApJ, 565, 244
 Harris, D. E., Krawczynski, H., & Taylor, G. B. 2002, ApJ, 578, 60
 Marshall, H. L., Miller, B. P., Davis, D. S., Perlman, E. S., Wise, M., Canizares, C. R., & Harris, D. E. 2002, ApJ, 564, 683
 Tavecchio, F., Maraschi, L., Sambruna, R. M., & Urry, C. M. 2000, ApJ, 544, 23
 Worrall, D. M., Birkinshaw, M., & Hardcastle, M. J. 2001, MNRAS, 326, L7